Applied Thermal Engineering 30 (2010) 1461–1469

Contents lists available at ScienceDirect

Applied Thermal Engineering

journal homepage: www.elsevier.com/locate/apthermeng

Numerical investigation of simultaneous heat and mass transfer mechanisms occurring in a gypsum board exposed to fire conditions

D. Kontogeorgos, M. Founti*

National Technical University of Athens, School of Mechanical Engineering, Laboratory of Heterogeneous Mixtures & Combustion Systems, Thermal Engineering Section, Heroon Polytechniou 9, Zografou Campus, 15780 Polytechnioupoli-Zografou, Athens, Greece

ARTICLE INFO

Article history:
Received 17 July 2009
Accepted 3 February 2010
Available online 10 March 2010

Keywords:
Gypsum
Dehydration
Transient heat mass transfer
Porous materials

ABSTRACT

This paper investigates the simultaneous heat and mass transfer mechanisms occurring in a gypsum board exposed to fire conditions. An in-house developed code (HETRAN), simulating heat and mass transfer in porous building materials, has been used to predict the heat and mass transfer characteristics within gypsum boards. The code solves numerically a set of mass and energy equations appropriate for the heat and mass transfer in porous materials, assuming homogeneity, local thermodynamic equilibrium and mass transfer due to diffusion and pressure gradients. The predicted temperature evolution within the gypsum sample, with and without mass transfer, is compared to experimental data, demonstrating that vapor migration through the sample holds a significant role in the board behavior under elevated temperatures. The results demonstrate that vapor migrates towards both directions of the board (fire and ambient side), with diffusion mass transfer being the dominant mass transfer mechanism, whereas air moves towards the "fire side". The dehydration front moves from the "fire side" to the ambient side, with a high velocity in the beginning, which reduces as the front moves through the gypsum sample to the ambient side.

1. Introduction

Simultaneous heat and mass transfer accompanied by phase change and/or heat absorption in porous materials is a process which frequently occurs in various engineering applications, such as drying processes [1–4], cooling procedures [5], building energy analysis [6–9], food industry [10], rock and soils mechanics [11] etc. Any porous building material consists of a solid, pore containing, matrix, which includes moisture (water vapor, absorbed or chemically bound water and ice) and dry air. The fluids in a porous material (gas and liquid) remain immiscible only if there are interfaces with non-zero surface tension. If the surface tension is zero, then the capillary pressure is zero, indicating equal pressure for both fluids [12]. Under internal heat generation conditions, the mass transfer mechanism is primarily through a total pressure and mass concentration gradient established due to the rapid vapor generation inside the material. Most of the moisture is vaporized before leaving the material. However, when the material is initially very wet and the pressure inside rises rapidly, liquid may be removed under the influence of pressure gradients before it is vaporized [10]. On the other hand, when the water content is quite small, the liquid water migration and the effect of liquid water migration on heat transfer are very small and can be neglected [13].

Gypsum is a porous material made of calcium sulphate and water. When it is subjected to sufficient heat, the absorbed (free) and the chemically bound water is released into the pores and begins to evaporate. During this process, the pressure within the pores is increased and in conjunction with temperature and mass concentration gradients, the gas mixture (water vapor and air) is transferred through the pores. The heat that is absorbed during the evaporation – dehydration process contributes to the fire resistance of gypsum [14]. In the context of building fire safety, gypsum plasterboards are capable of decelerating the penetration of fire through walls and floors, due to the endothermic gypsum dehydration process that takes place in high temperatures [15–18].

Several computational efforts have been made in the past to predict the thermal behavior of gypsum boards under fire conditions. Most of the researchers have performed only heat transfer calculations using an apparent specific heat in order to incorporate the dehydration process into the model [14–16,19–23] or the concept of moving dehydration front from the heated to the unheated side [24,25]. In the case of apparent specific heat, variations of specific heat peak width have been proven to have no effect on the temperature predictions. On the

* Corresponding author. Tel.: +30 210 772 3605; fax: +30 210 772 3527.
E-mail address: mfou@central.ntua.gr (M. Founti).

1359-4311/$ – see front matter © 2010 Elsevier Ltd. All rights reserved.
doi:10.1016/j.applthermaleng.2010.03.006

Nomenclature

$C_{p,g}^{(k)}$	constant pressure specific heat of the kth gas phase component, [J kg^{-1} K^{-1}]
C_s	specific heat of the solid component, [J kg^{-1} K^{-1}]
D_{AB}	binary diffusivity for system A–B, [m^2 s^{-1}]
D_{eff}	effective diffusion coefficient for porous materials, [m^2 s^{-1}]
h_c	heat transfer convection coefficient, [W m^{-2} K^{-1}]
h_m	mass transfer convection coefficient, [m s^{-1}]
$\mathbf{j}_{diff}^{(k)}$	mass flux vector of the kth gas phase component per unit area due to diffusion, [kg s^{-1} m^{-2}]
$\mathbf{j}_{pres}^{(k)}$	mass flux vector of the kth gas phase component per unit area due to pressure gradients, [kg s^{-1} m^{-2}]
k_{eff}	effective thermal conductivity for porous materials, [W m^{-1} K^{-1}]
K	permeability tensor, [m^2]
MW	molecular weight, [kg kmol^{-1}]
n	normal vector
N^g	number of gas phase components
P_g	total pressure of the gas phase mixture, [Pa]
Pr	Prandtl number
$\dot{Q}_M^{'''(k)}$	mass production/consumption of the kth gas phase component per unit volume, [kg s^{-1} m^{-3}]
$\dot{Q}_T^{'''}$	heat production/consumption per unit volume, [W m^{-3}]
R_g	universal gas constant, 8314, [J kmol^{-1} K^{-1}]
Sc	Schmidt number
t	simulation time, [s]
T	temperature, [K]
$u(t)$	velocity of the dehydration front, [m s^{-1}]
$\mathbf{U}_g^D$	Darcian velocity vector, [m s^{-1}]
x	space position vector, [m]
$\mathbf{X}_{BOUND}$	boundary node position vector, [m]
$x(t)$	position of the dehydration front, [m]
Y_{vapor}	vapor mass fraction, [kg kg^{-1}]

Greek symbols

ε	surface emissivity
μ_g	dynamic viscosity of the gas phase mixture, [Pa s]
$\rho_g^{(k)}$	mass concentration of the kth gas phase material, [kg m^{-3}]
ρ_s	density of the solid component, [kg m^{-3}]
σ	Stefan–Boltzmann constant, 5.67 × 10^{-8}, [W m^{-2} K^{-4}]
τ	tortuosity factor
ϕ	volume porosity

Subscripts

air	air
amb	ambient
g	gas
i	index for node numbering
mix	mixture
s	solid
w	wall

Superscripts

k	index for gas phase component numbering

Special symbols

d	total derivative operator
∂	partial derivative operator
∇	Nabla operator

other hand, variations of the specific heat peak temperatures have a considerable effect on the predictions of the temperature evolution [23]. In all these cases, the integral surface of the specific heat curves was maintained constant. Under fire conditions, the radiant heat transfer across the cavity of gypsum board assemblies and the gaps formed by the shrinkage of supporting wood stud cross sections play a very important role in the numerical predictions and they must taken be into consideration [19,20].

It is clear that a detailed combined heat and mass transfer analysis is needed to account for the vapor migration inside gypsum boards. The approach has been mainly applied in the modeling of concrete slabs [12,26–31], with few attempts reported for gypsum boards [18,32,33]. An indirect approach that allowed the use of only heat transfer analysis was developed by Ang and Wang [32,33]. The specific heat of dry gypsum has been artificially increased, over the temperature region of water evaporation, to values above the latent heat of evaporation, accounting for the heating rate applied in the gypsum board.

Macroscopic large scale fire experiments cannot shed light on the meso and micro scale time variation of porous material properties under fire conditions. Appropriate computational tools can effectively fill in this gap, support the understanding of porous material transient behavior – and in particular of gypsum boards – under fire conditions, as well as the development of new products with enhanced properties. In the current work, the simultaneous heat and mass transfer mechanisms occurring inside a gypsum board exposed to fire conditions are investigated. For this purpose, an updated version of the in-house developed code HETRAN [22] is used and the predictions of the temperature evolution within the gypsum samples, with and without mass transfer, are compared with the experimental data of Ghazi Wakili et al. [14], revealing the importance of vapor migration in the gypsum board behavior under elevated temperatures. Furthermore, mass concentration, mass flux and pressure distributions, inside the gypsum sample, depict that the vapor moves towards both directions, with the diffusion mass transfer being the dominant mass transfer mechanism, whereas the dehydration front is moving from the “fire side” to the ambient side.

1.1. Gypsum thermo-chemistry

Gypsum boards consist mainly of gypsum, which is a crystalline mineral of calcium sulphate combined with 21% by weight chemically bound water, known as calcium sulphate dehydrate ($CaSO_4 \cdot 2H_2O$). In addition, gypsum usually contains a small amount of absorbed free water, as well as calcium carbonate ($CaCO_3$). When gypsum is heated above 90 °C, the chemically bound water dissociates from the crystal lattice and evaporates. This process, known as “dehydration” or “calcination” of gypsum, takes place between 90 °C and 250 °C, depending on the heating rate, and requires the absorption of a large amount of heat. Heat transfer through the gypsum board is practically delayed until the calcination process is completed.

The dissociation of the chemical bound water takes place in two stages. In the first stage, the calcium sulphate dihydrate loses 75% of its water, thus forming calcium sulphate hemi-hydrate ($CaSO_4 \cdot 1/2H_2O$):

$$CaSO_4 \cdot 2H_2O + Q \leftrightarrow CaSO_4 \cdot \frac{1}{2}H_2O + \frac{3}{2}H_2O\uparrow \quad (1)$$

If gypsum is further heated, a second reaction occurs, where the calcium sulphate hemi-hydrate loses the remaining water to form the calcium sulphate anhydrate ($CaSO_4$):

$$CaSO_4\cdot\frac{1}{2}H_2O + Q \leftrightarrow CaSO_4 + \frac{1}{2}H_2O\uparrow \quad (2)$$

Both reactions are endothermic and absorb a large amount of energy, denoted by Q in eqs. (1) and (2). Several estimates Q can be found in the literature. Harmathy [34] calculated that the energy required to drive moisture off is 201 kJ/kg, which is low compared with that recommended by other authors. Andersson and Jansson [35] reported that the energy absorbed during the evaporation of the 75% of chemically bound water is 515 kJ/kg, whereas the remaining 25% of crystallization water needs 185 kJ/kg to dehydrate. Axenenko [24] theoretically calculated that the entire amount of energy required by the first and second dehydration reactions is 496 kJ/kg and 169 kJ/kg, respectively. Several researchers used Differential Scanning Calorimetry (DSC) at different scanning rates in order to measure the apparent specific heat and the dehydration energy. Mehaffey et al. [15] used DSC scanning rates of 2 and 20 °C/min and found that the dehydration energy is 500 kJ/kg. Ghazi Wakili et al. [14] used a scanning rate of 20 °C/min and measured the total dehydration energy to be 450 kJ/kg. Finally, Manzello et al. [18] used the same scanning rate and they found that the amount of energy absorbed by the first and second dehydration reaction is 390 kJ/kg and 180 kJ/kg, respectively. The differences are mainly associated with the different chemical composition – water content and other ingredients – of the gypsum board samples. The values of Ghazi Wakili et al. [14] have been used in the current study.

At temperatures near 400 °C, a third, slightly exothermic reaction occurs, in which the molecular structure of the soluble crystal irreversibly reorganizes itself into a lower insoluble energy state (hexagonal to orthorhombic) [17,18]:

$$CaSO_4(\text{sol}) \rightarrow CaSO_4(\text{insol}) + Q \quad (3)$$

The energy produced during this exothermic reaction, denoted as Q in eq. (3), was calculated from the apparent specific heat curves of Manzello et al. [18], by integrating the area under the specific heat peak value corresponding to this reaction, and found to be 34 kJ/kg.

A reduction of gypsum mass is observed at approximately 700 °C, corresponding to the decomposition of $CaCO_3$ [14]:

$$CaCO_3 + Q \rightarrow CaO + CO_2\uparrow \quad (4)$$

This step has not been identified by some authors [15] or has been incorrectly identified as the second dehydration step by others [24]. The decomposition of $CaCO_3$, eq. (4), is an endothermic process and the energy required, denoted as Q in eq. (4), is 200 kJ/kg, as reported in Ghazi Wakili et al. [14], corresponding to 10% of the carbonate fraction in the gypsum. The value of the endothermic energy needed for the decomposition of pure carbonate reported to be ~2000 kJ/kg in the work of Sanders and Gallagher [36] and Maciejewski [37].

2. Mathematical modeling

The in-house developed HETRAN code [22] was extended to take into account gas phase transport through a porous material (vapor migration within a gypsum board in this case). The software solves numerically a set of mass and energy equations appropriate for the heat and mass transfer in porous materials, assuming homogeneity, local thermodynamic equilibrium and mass transfer due to diffusion and pressure gradients.

Table 1
Variables and coefficients of the generalized conservation eq. (9).

f	A_f	B_f	$\mathbf{C}_f$	Q_f
$\rho_g^{(k)}$	ϕ	D_{eff}	$\mathbf{U}_g^D$	$\dot{Q}_M^{'''(k)}$
T	$(1-\phi)\rho_s C_s + \phi\sum_{k=1}^{N^g}\rho_g^{(k)}C_{p,g}^{(k)}$	k_{eff}	$\sum_{k=1}^{N^g}\left\{C_{p,g}^{(k)}\left(\mathbf{j}_{\text{diff}}^{(k)}+\mathbf{j}_{\text{pres}}^{(k)}\right)\right\}$	$\phi\frac{\partial P_g}{\partial t}+\dot{Q}_T^{'''}$

2.1. Mass conservation of species

The governing equation for the mass conservation of N^g gas phase components in a porous material accounts for diffusion (Fick's law) and pressure gradients (Darcy's law):

$$\phi\frac{\partial\rho_g^{(k)}}{\partial t} = \nabla\bullet\left(D_{\text{eff}}\nabla\rho_g^{(k)}\right) - \nabla\bullet\left(\mathbf{U}_g^D\rho_g^{(k)}\right) + \dot{Q}_M^{'''(k)} \quad (5)$$

2.2. Momentum conservation (Darcy's law)

The mean filtration velocity field of the gas phase mixture is calculated from the Darcy's law:

$$\mathbf{U}_g^D = -\frac{\mathbf{K}}{\mu_g}\nabla P_g \quad (6)$$

The gaseous phase consists of ideal gases, where the gas mixture pressure is the summation of each components partial pressure.

2.3. Energy conservation

The energy balance shows that heat is transferred through conduction, diffusion and pressure gradients of the gas phase mixture, while there is energy production/consumption due to pressure changes and other energy sources i.e. phase change:

$$\left((1-\phi)\rho_s C_s + \phi\sum_{k=1}^{N^g}\rho_g^{(k)}C_{p,g}^{(k)}\right)\frac{\partial T}{\partial t} = \nabla\bullet\left(k_{\text{eff}}\nabla T\right) - \nabla\bullet\left(\left[\sum_{k=1}^{N^g}\left\{C_{p,g}^{(k)}\left(\mathbf{j}_{\text{diff}}^{(k)}+\mathbf{j}_{\text{pres}}^{(k)}\right)\right\}\right]T\right) + \phi\frac{\partial P_g}{\partial t} + \dot{Q}_T^{'''} \quad (7)$$

The mass fluxes due to diffusion and convection contained in energy equation are calculated from Fick's and Darcy's law:

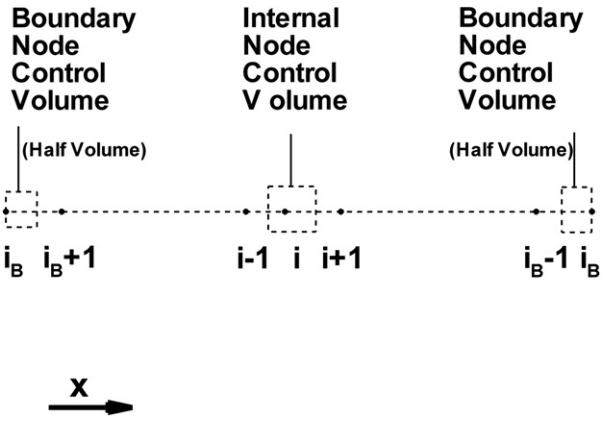

Fig. 1. Control volumes.

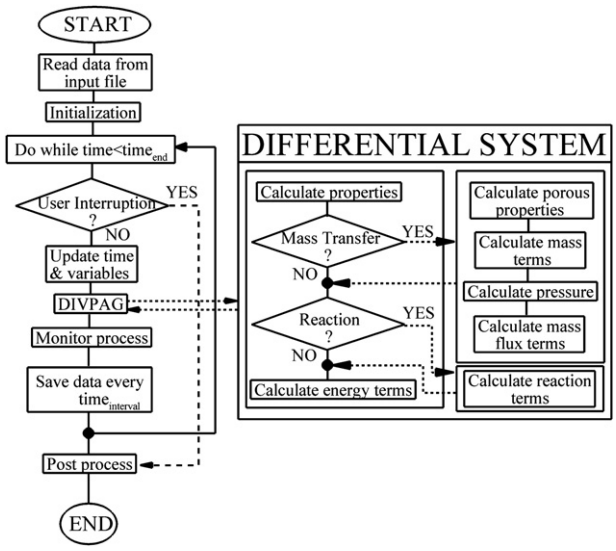

Fig. 2. Flow chart diagram of HETRAN code.

$$\begin{aligned}\mathbf{j}_{\text{pres}}^{(k)} &= \rho_{\text{g}}^{(k)}\mathbf{U}_{\text{g}}^{\text{D}} \\ \mathbf{j}_{\text{diff}}^{(k)} &= -D_{\text{eff}}\nabla\rho_{\text{g}}^{(k)}\end{aligned} \tag{8}$$

3. Numerical analysis

The conservation equations can be summarized into one general equation:

$$A_{\text{f}}\frac{\partial f}{\partial t} = \nabla\bullet\left(\mathbf{B}_{\text{f}}\nabla f\right) - \nabla\bullet\left(\mathbf{C}_{\text{f}}f\right) + Q_{\text{f}} \tag{9}$$

Table 1 summarizes the variables and coefficients used in each conservation equation.

3.1. Spatial discretization

Finite volume techniques [38] are used to solve the 1-D balance equations, where eq. (9) is integrated over the finite volume shown in Fig. 1. The domain is divided into $N-1$ cells bounded by N nodes. The variable is defined on the nodes and the control volumes are determined from the half – cells surrounding the nodes. The spatial discretization is defined from:

$$\frac{\mathrm{d}f_i}{\mathrm{d}t} = \frac{C_{\text{B,i}}^{\text{f}} + C_{\text{C,i}}^{\text{f}} + C_{\text{Q,i}}^{\text{f}}}{C_{\text{A,i}}^{\text{f}}} \tag{10}$$

where

$$\begin{aligned}C_{\text{B,i}}^{\text{f}} &= \left\{B_{\text{f},i+1/2}\frac{f_{i+1}-f_i}{x_{i+1}-x_i} - B_{\text{f},i-1/2}\frac{f_i-f_{i-1}}{x_i-x_{i-1}}\right\} \\ C_{\text{C,i}}^{\text{f}} &= -\left\{C_{\text{f},x,i+1/2}\frac{f_{i+1}+f_i}{2} - C_{\text{f},x,i-1/2}\frac{f_i+f_{i-1}}{2}\right\} \\ C_{\text{Q,i}}^{\text{f}} &= \left\{Q_{\text{f},i+1/2}\frac{x_{i+1}-x_i}{2} + Q_{\text{f},i-1/2}\frac{x_i-x_{i-1}}{2}\right\} \\ C_{\text{A,i}}^{\text{f}} &= \left\{A_{\text{f},i+1/2}\frac{x_{i+1}-x_i}{2} + A_{\text{f},i-1/2}\frac{x_i-x_{i-1}}{2}\right\}\end{aligned}$$

3.2. Solver algorithm

The set of equations can be summarized into one ordinary differential system:

$$\frac{\mathrm{d}\mathbf{f}}{\mathrm{d}t} = \mathbf{f}(t,\mathbf{f}) \tag{11}$$

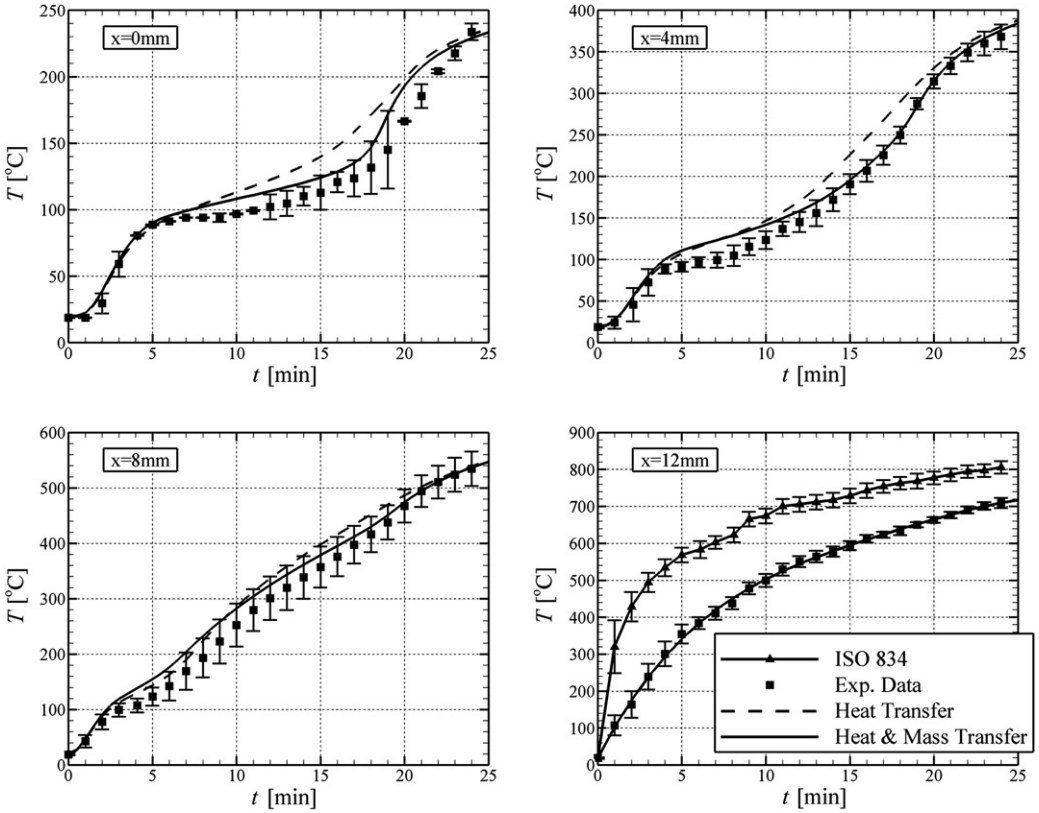

Fig. 3. Comparison between HETRAN predictions (with and without mass transfer) and experimental data [14] of the temperature evolution inside the gypsum board.

where

$$\mathbf{f} = \begin{Bmatrix} \mathbf{T} \\ \boldsymbol{\rho}_g^{(k)} \end{Bmatrix} \text{ and } \mathbf{f}(t,\mathbf{f}) = \begin{Bmatrix} \mathbf{f}_T \\ \mathbf{f}_M^{(k)} \end{Bmatrix}, k = 1 \ldots N^g, \text{ with the vectors } \mathbf{T}, \mathbf{F}_T, \boldsymbol{\rho}_g^{(k)} \text{ and } \mathbf{f}_M^{(k)} \text{ being}$$

$$\mathbf{T} = \begin{Bmatrix} T_1 \\ \vdots \\ T_i \\ \vdots \\ T_N \end{Bmatrix}, \quad \mathbf{f}_T = \begin{Bmatrix} \frac{C^T_{B,1}+C^T_{C,1}+C^T_{Q,1}}{C^T_{A,1}} \\ \vdots \\ \frac{C^T_{B,i}+C^T_{C,i}+C^T_{Q,i}}{C^T_{A,1}} \\ \vdots \\ \frac{C^T_{B,N}+C^T_{C,N}+C^T_{Q,N}}{C^T_{A,N}} \end{Bmatrix}, \quad \boldsymbol{\rho}_g^{(k)} = \begin{Bmatrix} \rho^{(k)}_{g,1} \\ \vdots \\ \rho^{(k)}_{g,i} \\ \vdots \\ \rho^{(k)}_{g,N} \end{Bmatrix} \text{ and}$$

$$\mathbf{f}_M^{(k)} = \begin{Bmatrix} \frac{C^{\rho_g^{(k)}}_{B,1}+C^{\rho_g^{(k)}}_{C,1}+C^{\rho_g^{(k)}}_{Q,1}}{C^{\rho_g^{(k)}}_{A,1}} \\ \vdots \\ \frac{C^{\rho_g^{(k)}}_{B,i}+C^{\rho_g^{(k)}}_{C,i}+C^{\rho_g^{(k)}}_{Q,i}}{C^{\rho_g^{(k)}}_{A,1}} \\ \vdots \\ \frac{C^{\rho_g^{(k)}}_{B,N}+C^{\rho_g^{(k)}}_{C,N}+C^{\rho_g^{(k)}}_{Q,N}}{C^{\rho_g^{(k)}}_{A,N}} \end{Bmatrix}$$

In order to solve the set of equations described, Gear's Backward Differentiation Formula (BDF) method [39], with automatic control of step size and order, is used. Fig. 2 presents the "HETRAN" code flow chart diagram.

4. Results and discussion

In order to validate the HETRAN code, predictions are compared with experimental data from Ghazi Wakili et al. [14], where a gypsum board plate of size 1.25 m × 1.05 m × 0.012 m was subjected to the standard ISO 834 fire [40]. A 12 mm thick solution domain, with heat and mass boundary conditions allocated to each boundary node, was simulated. The pressure along the boundaries is considered to be atmospheric and the mass flow at all boundaries is specified as diffusive-convective mass flow [30,32,33].

In the ambient side it is assumed that the air temperature is 20 °C and relative humidity 40%. In this case, the mass boundary condition for vapor is a convection boundary condition (eq. (12)), whereas the heat boundary condition is a convection − radiation boundary condition (eq. (13)).

$$\left(\mathbf{j}^{(\text{vapor})}_{\text{diff}} + \mathbf{j}^{(\text{vapor})}_{\text{pres}}\right) \bullet \mathbf{n}|_{\mathbf{x}=\mathbf{x}_{\text{BOUND}}} = h_m\left(\rho^{(\text{vapor})}_{g,\text{amb}} - \rho^{(\text{vapor})}_{g,w}\right) \quad (12)$$

$$-k_{\text{eff}}\nabla T \bullet \mathbf{n}|_{\mathbf{x}=\mathbf{x}_{\text{BOUND}}} = h_c(T_{\text{amb}} - T_w) + \varepsilon\sigma\left(T^4_{\text{amb}} - T^4_w\right) \quad (13)$$

The mass concentration of air at the boundary is calculated via Dalton's law. The heat transfer convection coefficient and the emissivity were chosen to be $h_c = 10$ W/m^2/K and $\varepsilon = 0.9$, respectively, while the mass transfer convection coefficient was chosen to be $h_m = 9.55 \times 10^{-3}$ m/s, calculated from $h_m = 1/(\rho_{air}C_{p,air}) \times (\text{Pr}/\text{Sc})^{2/3} \times h_c$ [30], with all the variables in this equation taken at ambient temperature.

For the "fire side", the measured temperature on the surface of the sample was used as wall temperature boundary condition, thus avoiding inaccuracies involved in the procedure of defining the convective and radiative heat transfer due to the experimental enclosure-furnace [41]. Assuming that the fuel is methane, the vapor mass fraction inside the furnace was calculated, from the stoichiometric combustion of methane, to be $Y_{\text{vapor}} = 0.1239$. The vapor mass concentration inside the furnace was calculated from:

$$\rho_{\text{vapor}}(t) = Y_{\text{vapor}}\rho_{\text{mix}} = Y_{\text{vapor}}\frac{P_{\text{amb}}\text{MW}_{\text{mix}}}{R_g T_{\text{fire}}(t)} \quad (14)$$

The physical properties of the simulated gypsum board were taken from the literature. The porosity, the permeability and the diffusion coefficients were chosen to be $\phi = 0.68$ [42] and $K = 10^{-15}$ m^2 [43] (similar to sandstone), $D_{eff} = \phi D_{AB}/\tau$ [44] and $\tau = 1.869$ [44]. The diffusion coefficient of water vapor in air was chosen to be $D_{AB} = 2.56 \times 10^{-5}$ m^2 [45]. The rate of vapor production inside the gypsum sample was calculated from the TGA curve provided from literature [14]. The rest of the physical properties, i.e. density, specific heat and thermal conductivity were also taken from literature [14].

The total number of nodes used in the simulation was 61, giving a mesh step $\delta x = 0.2$ mm, while the time step was $\delta t = 0.005$ s, with an accuracy of 10^{-7}. Mesh and time solution independence was verified using double number of nodes and half time step, where the computational results showed no difference. The CPU time consumed on an Intel Core 2 Duo 1.8 GHz, 2 GB was 13 h, 23 min and 44 s.

4.1. Temperature predictions

In Fig. 3, HETRAN predictions, with and without mass transfer, of the temperature evolution inside the gypsum board are compared with the experimental data of Ghazi Wakili et al. [14] (position $x = 0$ mm corresponds to the ambient side, whereas position

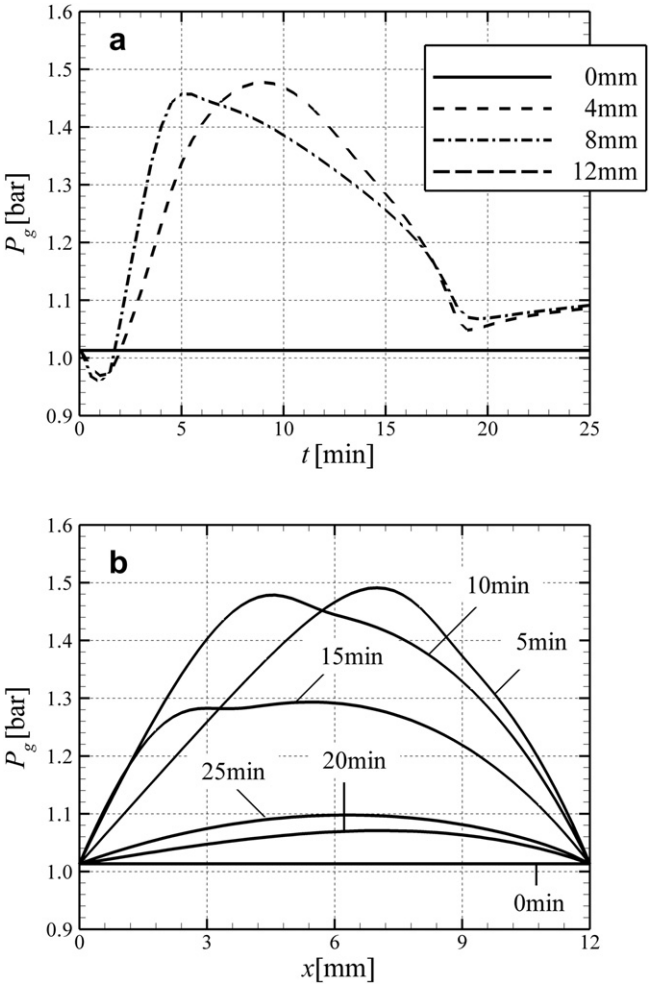

Fig. 4. a) Time evolution of gas phase mixture total pressure at different positions inside the gypsum sample and b) spatial distribution of gas phase mixture total pressure at different time steps inside the gypsum sample.

$x = 12$ mm corresponds to the "fire side"). As it is shown, including mass transfer in the model improves agreement with the experimental data, in comparison to the heat transfer calculations. The observed small over prediction of the calculated temperature field with the combined heat and mass transfer mechanisms can be associated to the fact that the mass transfer physical properties, i.e. porosity, permeability, diffusion coefficient, mass transfer coefficient etc, are temperature dependent, which is not taken into account in this investigation. Numerical experiments using variable specific heat values indicate that the additional amount of energy offered to the dehydration process due to mass transfer amounts approximately to 191 kJ/kg (~42% increase of the dehydration energy of 450 kJ/kg measured in [14]), which is very close to the ~45% estimated in the work of Ang & Wang [33].

4.2. Pressure predictions

In Fig. 4, the time and spatial distribution of the gas phase mixture (air and vapor) total pressure is presented. The initial under-pressure shown in Fig. 4a indicates that fresh air is sucked in the sample during the time period that precedes dehydration, which is characterized by a continuous temperature rise and decrease of the air mass concentration within the sample. It is clear that pressure starts increasing when the dehydration process begins (~100 °C and after the first 2 min from the beginning of the experiment) and attains local maximum values after 5–10 min from the beginning of the exposure of the sample to the fire (Fig. 4a, $x = 4$ mm and $x = 8$ mm). Fig. 4b presents the spatial distribution of pressure within the sample and confirms that pressure increases from the fire side (Fig. 4b, $x = 0.012$ m) towards the ambient (Fig. 4b, $x = 0$ m).

At temperatures around 100 °C, the chemically bound water starts to be released into the pores and begins to evaporate. During the evaporation process, pore pressure is increased and pressure gradients are developed inside the gypsum sample. The maximum pressure values achieved are almost 1.5 atm (Fig. 4a and b), with the pressure at the boundaries set to 1 atm, leading to ca. 0.5 atm overpressure.

After completion of the dehydration process the pores of the sample re-filled and saturated with air (as confirmed by Fig. 6a). The observed trend of a relative small increase in the local pressure (Fig. 4a, $t > 20$ min) is due to a combined change in the air mass concentration and temperature, which cannot be anticipated on the basis of gas equation of state.

4.3. Mass flux predictions

Fig. 5 illustrates the time distributions of the gas phase components (air and vapor) mass fluxes. Diffusive (j_{diff}) and pressure gradient (j_{pres}) mass fluxes are compared in the left hand and right hand columns respectively, for air (1st row) and vapor (2nd row). Overall, it can be observed that the pressure gradient term attains much lower values than diffusive mass transfer. Positive values indicate movement towards the "fire side" and vice versa. Air diffuses only to the "fire side" (Fig. 5a), due to the fact that in the "fire side" there are only combustion products and no air. Thus, in one hand, air diffuses from higher concentrations (ambient side) to lower concentrations ("fire side"). On the other hand, pressure gradients force air to move towards both directions (Fig. 5b). Nevertheless, the resultant direction of the air movement (summation of diffusive and pressure gradient flux) is from the ambient side to the "fire side", concluding that diffusion is the dominant mass transfer mechanism for air.

During the evaporation process, water vapor is released and pore pressure is increased creating vapor concentration and pressure gradients, leading water vapor to the boundaries of the

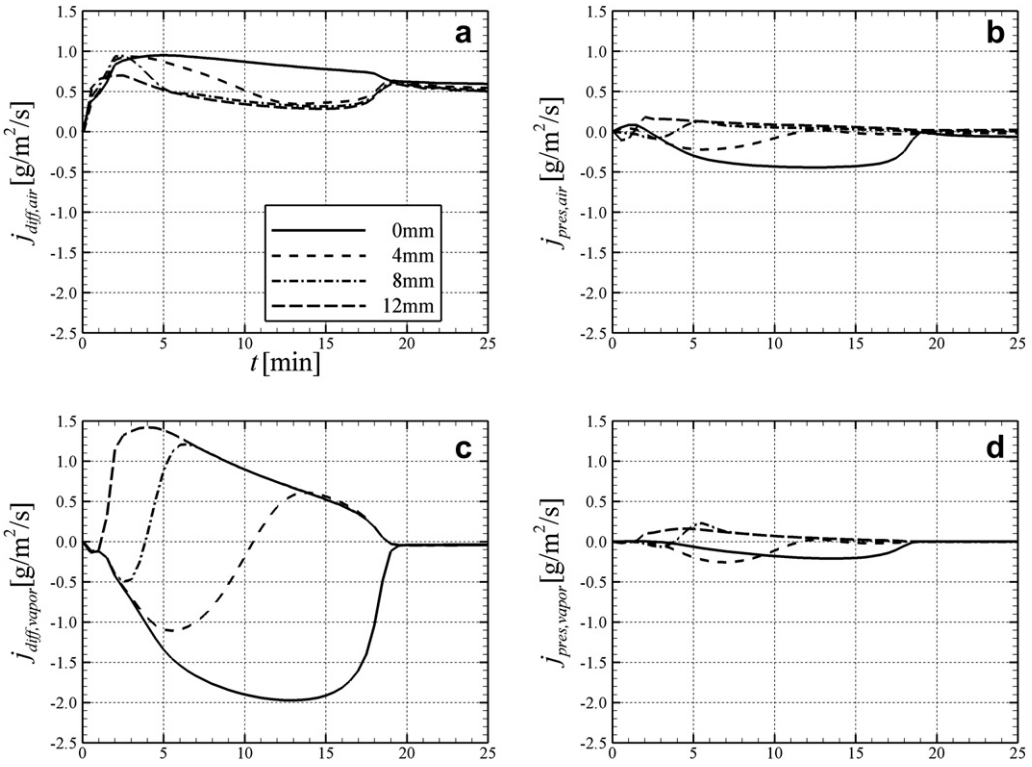

Fig. 5. Time evolution of a) air diffusive ($j_{diff,air}$), b) air pressure gradient ($\mathbf{j}_{pres,air}$), c) vapor diffusive ($\mathbf{j}_{diff,vapor}$) and d) vapor pressure gradient ($\mathbf{j}_{pres,vapor}$) mass fluxes at different positions inside the gypsum sample.

gypsum sample. This is clearly shown in Fig. 5c and d, where some of the vapor migrates to the "fire side". Simultaneously, an amount of vapor is driven to the ambient side of the sample, where it condenses into liquid (condensation is not taken into account in the current version of the model). Despite the fact that water vapor diffuses in both directions within the sample (Fig. 5c), it can be noted that in the boundaries it diffuses only outwards. Finally, it can be seen that diffusive water vapor flux (Fig. 5c) is almost one order of magnitude higher than the water vapor flux due to pressure gradients (Fig. 5d), concluding that diffusion is the dominant mass transfer mechanism for water vapor.

4.4. Mass concentration predictions

Fig. 6 depicts the time evolution of the mass concentration of the gas phase components (air and vapor). Water vapor is released during the dehydration process with increasing mass concentration within the sample (Fig. 6b), while the air mass concentration decreases inside the gypsum sample (Fig. 6a). By comparing Fig. 6a and b, it can be observed that when all the water vapor is driven out from the sample (after ca. 18.5 min), the pores are filled again with air and the air mass concentration is increased.

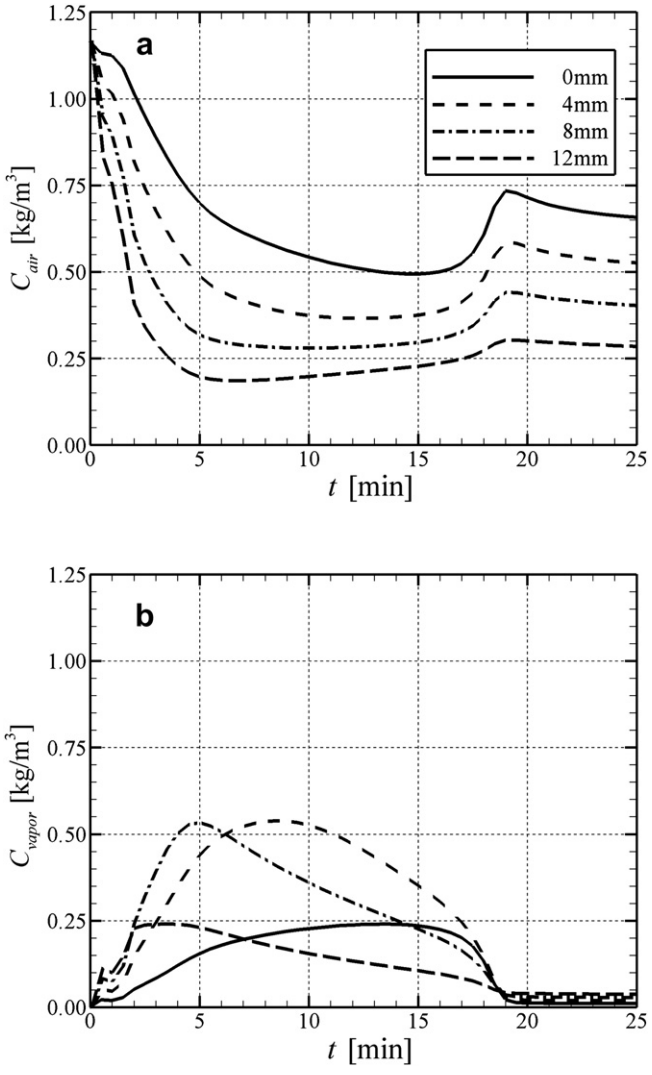

Fig. 6. Time evolution of a) air and b) vapor mass concentration at different positions inside the gypsum sample.

It can be seen from Fig. 7 that the position of the dehydration front, $x(t)$, defined as the location of the maximum water vapor concentration at a specific time step, moves from the "fire side" ($x = 0.012$ m) towards to the ambient side ($x = 0$ m). The dehydration process starts when the temperature in the exposed side reaches 100 °C (after ~1.5 min from the beginning of the specific application) and ends when all the chemically bound water is evaporated (after ~18.5 min). Finally, the dehydration front velocity, $u(t)$, defined from the derivative of the dehydration front position, is high in the beginning of the phenomenon due to the high heat flux from the "fire side", leading to high evaporation rates, and decreases gradually as the front moves to the ambient side, due to the reduction of the heat flux.

4.5. Heat flux predictions

Fig. 8 illustrates the heat flux distributions inside the gypsum board at different time steps in the case of sole heat transfer (HT), where only heat conduction takes place, and in the case of simultaneous heat and mass transfer (HMT). In the former case, heat transfer is due to conduction ($q_{cond,HT}$). On the other hand, in the case of simultaneous heat and mass transfer, the heat flux can be analyzed into three different components; heat flux due to conduction ($q_{cond,MT}$), due to mass diffusion ($q_{diff,MT}$) and due to pressure gradients ($q_{pres,MT}$) of the gas phase mixture (air and vapor). It is obvious that the migration of the gaseous mixture has a significant impact on the overall heat flux ($q_{total,MT}$), defined as the sum of the above three components.

Fig. 9 visualizes representative heat flux vectors in two different positions inside the gypsum sample, behind (position b_{DF}) and in front (position u_{DF}) of the dehydration front. In the case of simultaneous heat and mass transfer, behind the dehydration front (position b_{DF}), the gas phase mixture moves towards the "fire side" transferring an amount of energy ($q_{diff,MT} + q_{pres,MT}$), while the conductive heat flux is transferred from the "fire side" to the ambient. Thus, the overall heat flux, which is the vector summation of the three heat flux components, is lower than in the case of sole heat transfer, leading to smaller temperature rise in this area and longer temperature plateau. On the other hand, in the case of

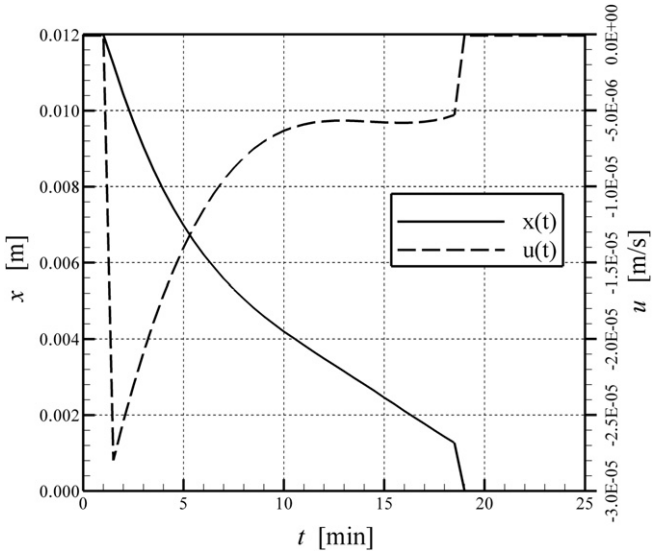

Fig. 7. Time evolution of the dehydration front position, $x(t)$ and velocity, $u(t)$.

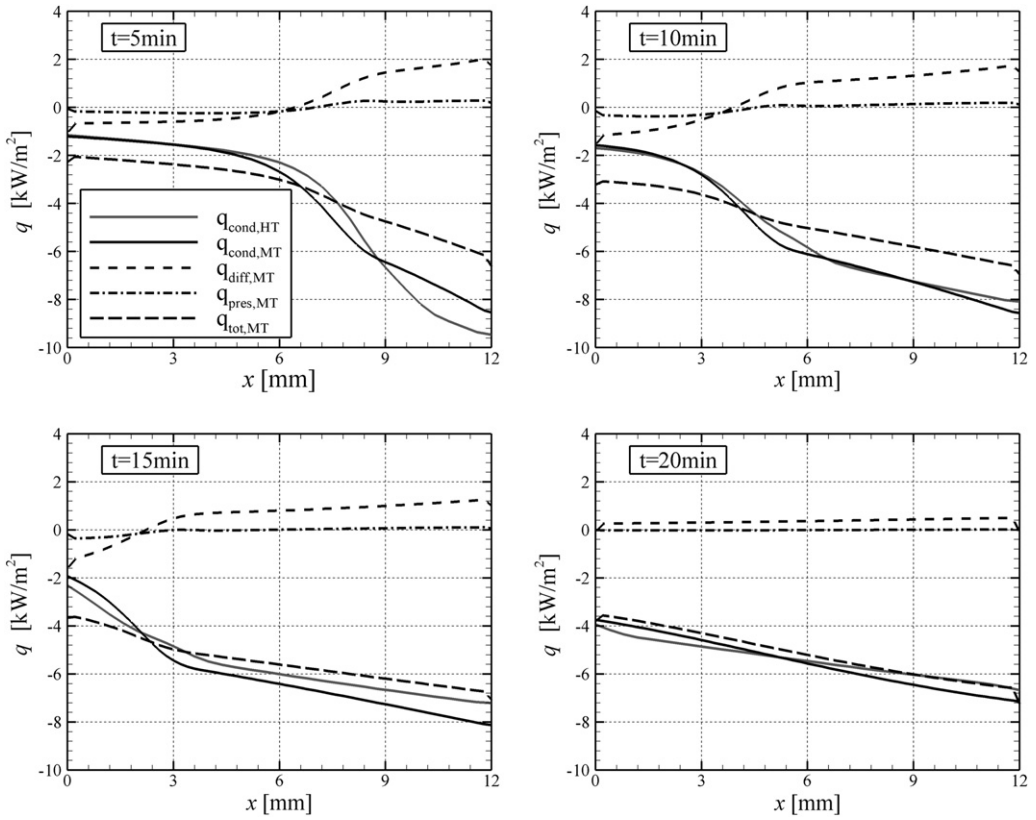

Fig. 8. Spatial distribution of heat flux inside the gypsum board at different time steps in the case of sole heat transfer and in the case of simultaneous heat and mass transfer.

simultaneous heat and mass transfer, in front of the dehydration front (position u_{DF}), the gaseous mixture moves towards the same direction as the conductive heat flux, with a positive contribution to the overall heat flux. Finally, when the dehydration process is completed, the total heat flux in case of simultaneous heat and mass transfer is smaller than the heat flux in case of sole heat transfer due to "fresh" air migration from the ambient side to the "fire side", as also shown in Fig. 8.

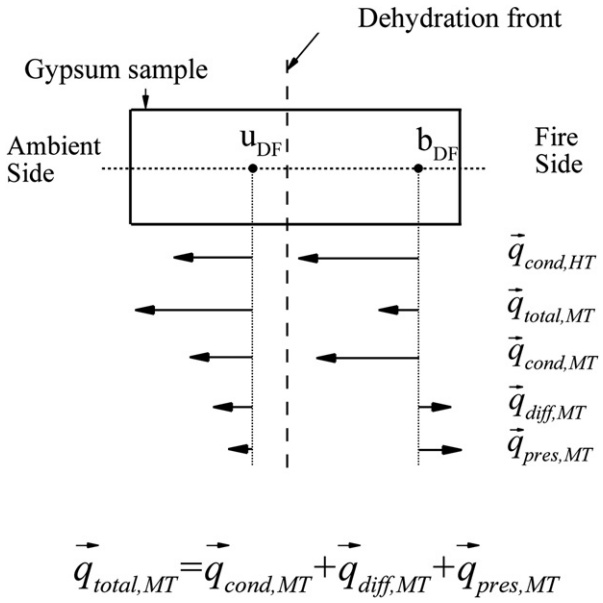

Fig. 9. Representative heat flux vectors behind and in front of the dehydration front.

5. Conclusions

In this paper, the simultaneous heat and mass transfer mechanisms occurring inside a commercial gypsum board exposed to fire conditions has been investigated. A combined heat and mass transfer model in porous building materials, assuming homogeneity, local thermodynamic equilibrium and mass transfer due to concentration and pressure gradients, has been developed and implemented. Predictions of the temperature evolution inside the gypsum sample, with and without mass transfer, have been compared with experimental data, depicting that mass transfer is a crucial mechanism that should be taken into account in numerical simulations. The numerical predictions have served to shed light in the mass and heat transfer phenomena occurring during the heating up of gypsum boards under fire conditions. It has been shown that the vapor released due to the dehydration process, fills in the pores and induces concentration and pressure gradients (max. 0.5 atm), which force water vapor to move towards both directions, affecting the temperature field inside the gypsum board. Results showed that the dominant mass transfer mechanism for the air and water vapor migration is the diffusion. Also, it has been shown that the dehydration front moves from the "fire side" to the ambient side, initially with a high velocity, due to the high heat flux from the "fire side", which decreases as the front moves towards to the ambient side. Finally, the overall heat flux in the case of simultaneous heat and mass transfer is smaller than the conductive heat flux in the case of heat transfer behind the dehydration front, leading to smaller temperature rise in this area and longer temperature plateau.

Acknowledgements

The authors acknowledge the financial support of the EC within the frame of the NMP FP6 IP – ISSB Project, Proposal No. 026661-2.

References

[1] Win-Jin Chang, Cheng-I Weng, An analytical solution to coupled heat and moisture diffusion transfer in porous materials. International Journal of Heat and Mass Transfer 43 (2000) 3621–3632.

[2] W.R. Foss, C.A. Bronkhorst, K.A. Bennett, Simultaneously heat and mass transport in paper sheets during moisture sorption from humid air. International Journal of Heat and Mass Transfer 46 (2003) 2875–2886.

[3] P. Salagnac, P. Glouannec, D. Lecharpentier, Numerical modeling of heat and mass transfer in porous medium during combined hot air, infrared and microwaves drying. International Journal of Heat and Mass Transfer 47 (2004) 4479–4489.

[4] T. Lu, S.Q. Shen, Numerical and experimental investigation of paper drying: heat and mass transfer with phase change in porous media. Applied Thermal Engineering 27 (2007) 1248–1258.

[5] Y.H. Andoh, B. Lips, Prediction of porous walls thermal protection by effusion or transpiration cooling. An analytical approach. Applied Thermal Engineering 23 (2003) 1947–1958.

[6] N. Mendes, P.C. Philippi, R. Lamberts, A new mathematical method to solve highly coupled equations of heat and mass transfer in porous media. International Journal of Heat and Mass Transfer 45 (2002) 509–518.

[7] R.C. Gaur, N.K. Bansal, Effect of moisture transfer across building components on room temperature. Building and Environment 37 (2002) 11–17.

[8] Gerson H. dos Santos, Nathan Mendes, Simultaneous heat and moisture transfer in soils combined with building simulation. Energy and Buildings 38 (2006) 303–314.

[9] M. Qin, R. Belarbi, A. Ait-Mokhtar, L. Nilsson, Coupled heat and moisture transfer in multi-layer building materials. Construction and Building Materials 23 (2009) 967–975.

[10] D.D. Dincov, K.A. Parrott, K.A. Pericleous, Heat and mass transfer in two-phase porous materials under intensive microwave hating. Journal of Food Engineering 65 (2004) 403–412.

[11] J. Rutqvist, Y.-S. Wu, C.-F. Tsang, G. Bodvarsson, A modeling approach for analysis of coupled multiphase fluid flow, heat transfer, and deformation in fractured porous rock. International Journal of Rock Mechanics and Mining Science 39 (2002) 429–442.

[12] B.A. Schrefler, F. Pesavento, Multiphase flow in deforming porous material. Computers and Geotechnics 31 (2004) 237–250.

[13] Z.Q. Chen, M.H. Shi, Study of heat and moisture migration properties in porous building materials. Applied Thermal Engineering 25 (2005) 61–71.

[14] K. Ghazi Wakili, E. Hugi, L. Wullschleger, T. Frank, Gypsum board in fire – modeling and experimental validation. Journal of Fire Sciences 25 (2007) 267–282.

[15] J.R. Mehaffey, P. Cuerrier, G. Carisse, A model for predicting heat transfer through gypsum-board/wood-stud exposed to fire. Fire and Materials 18 (1994) 297–305.

[16] M.A. Sultan, A model for predicting heat transfer through noninsulated unloaded steel-stud gypsum board wall assemblies exposed to fire. Fire Technology 32 (1996) 239–259.

[17] S.L. Manzello, R.G. Gann, S.R. Kukuck, K. Prasad, W. Jones, Performance of a non-load-bearing steel stud gypsum board wall assembly: experiments and modelling. Fire and Materials 31 (2007) 297–310.

[18] S.L. Manzello, R.G. Gann, S.R. Kukuck, B.L. David, Influence of gypsum board type (X or C) on real fire performance of partition assemblies. Fire and Materials 31 (2007) 425–442.

[19] H. Takeda, J.R. Mehaffey, WALL2D: a model for predicting heat transfer through wood-stud walls exposed to fire. Fire and Materials 22 (1998) 133–140.

[20] P. Clancy, Advances in modelling heat transfer through wood framed walls in fire. Fire and Materials 25 (2001) 241–254.

[21] G. Thomas, Thermal properties of gypsum plasterboard at high temperatures. Fire and Materials 26 (2002) 37–45.

[22] D.A. Kontogeorgos, D.I. Kolaitis, M.A. Founti, Numerical modelling of heat transfer in gypsum plasterboards exposed to fire, in: Proceedings of 6th International Conference on Heat Transfer. Fluid Mechanics and Thermodynamics, Pretoria, South Africa, 30 June to 2 July 2008 Paper Number KD1.

[23] L. Wullschleger, K. Ghazi Wakili, Numerical parameter study of the thermal behavior of a gypsum plaster board at fire temperatures. Fire and Materials 32 (2007) 103–119.

[24] O. Axenenko, G. Thorpe, The modelling of dehydration and stress analysis of gypsum plasterboards exposed fire. Computational Material Science 6 (1996) 281–294.

[25] J.R. McGraw, F.W. Mowrer, Flammability and dehydration of painted gypsum wallboard subjected to fire heat fluxes, fire safety science, in: Proceedings of the 6th International Symposium. International Association for Fire Safety Science, Poitiers, France, 5–9 July 1999 Paper number 1003.

[26] C.L.D. Huang, Multi-phase moisture transfer in porous media subjected to temperature gradient. International Journal of Heat and Mass Transfer 22 (1979) 1295–1307.

[27] C.L.D. Huang, H.H. Siang, C.H. Best, Heat and moisture transfer in concrete slabs. International Journal of Heat and Mass Transfer 22 (1979) 257–266.

[28] A. Bazant, J.C. Chern, W. Thonguthai, Finite element program for moisture and heat transfer in heated concrete. Nuclear Engineering and Design 68 (1981) 61–70.

[29] A. Dayan, Heat and mass transfer within an intensely heated concrete slab. International Journal of Heat and Mass Transfer 25 (10) (1982) 1461–1467.

[30] N.G. Ahmed, J. Hurst, Coupled heat and mass transport phenomena in siliceous aggregate concrete slabs subjected to fire. Fire and Materials 21 (1997) 161–168.

[31] J. Stakulcharoen, W. Pakdee, P. Ratanadecho, Analysis of transport phenomena in concrete walls exposed to hot gas, The 20th Conference of Mechanical Engineering Network of Thailand, Nakhon Ratchasima, Thailand 18–20 October 2006.

[32] C.N. Ang, Y.C. Wang, The effect of water movement on specific heat of gypsum plasterboard in heat transfer analysis under natural fire exposure. Construction and Building Materials 18 (2004) 505–515.

[33] C.N. Ang, Y.C. Wang, Effect of moisture transfer on specific heat of gypsum plasterboard at high temperatures. Construction and Building Materials 23 (2009) 675–686.

[34] T.Z. Harmathy, The SFPE Handbook of Fire Protection Engineering. Section 1 Chapter 26. Society of Fire Protection Engineers/National Fire Protection Association, Boston, 1988.

[35] L. Andersson, B. Jansson, Analytical Fire Design with Gypsum – A Theoretical and Experimental Study. Institute of Fire Safety Design, Lund, 1987.

[36] J.P. Sanders, P.K. Gallagher, Kinetic analyses using simultaneous TG/DSC measurements part I: decomposition of calcium carbonate in argon. Thermochimica Acta 388 (1–2) (2002) 115–128.

[37] M. Maciejewski, Computational aspects of kinetic analysis. Part B: the ICTAC kinetic project – the decomposition kinetics of calcium carbonate revisited, or some tips on survival in the kinetic minefield. Thermochimica Acta 355 (1–2) (2000) 145–154.

[38] S.V. Patankar, Numerical Heat Transfer and Fluid Flow. Hemisphere, London, 1980.

[39] C.W. Gear, Numerical Initial Value Problems in Ordinary Differential Equations. Prentice-Hall, Englewood Cliffs, New Jersey, 1971.

[40] International Standard ISO 834-1, Fire Resistance Tests – Elements of Building Construction – Part 1: General Requirements. International Standard ISO 834-1, 1999.

[41] U. Wickström, Heat transfer by radiation and convection in fire testing. Fire and Materials 28 (2004) 411–415.

[42] S.T. Craft, B. Isgor, G. Hadjisophocleous, J.R. Mehaffey, Predicting the thermal response of gypsum board subjected to a constant heat flux. Fire and Materials 32 (2008) 333–355.

[43] J. Bear, Dynamics of Fluids in Porous Media. Dover Publications, 1972.

[44] P. Blondeau, A.L. Tiffonnet, A. Damian, O. Amiri, J.L. Molina, Assessment of contaminant diffusivities in building materials from porosimetry tests. Indoor Air 13 (2003) 302–310.

[45] F.A. Schwertz, Jeanne E. Brow, Diffusivity of water vapor in some common gases. The Journal of Chemical Physics 19 (5) (1951) 640–646.